# Stagnant Mobile Phase Mass Transfer in Chromatographic Media: Intraparticle Diffusion and Exchange Kinetics

**ARTICLE** *in* THE JOURNAL OF PHYSICAL CHEMISTRY B · SEPTEMBER 1999

Impact Factor: 3.3 · DOI: 10.1021/jp990828b · Source: OAI

# Stagnant Mobile Phase Mass Transfer in Chromatographic Media: Intraparticle Diffusion and Exchange Kinetics

**Ulrich Tallarek,* Frank J. Vergeldt, and Henk Van As**

*Laboratory of Molecular Physics and Wageningen NMR Centre, Department of Biomolecular Sciences, Wageningen Agricultural University, Dreijenlaan 3, 6703 HA Wageningen, The Netherlands*

*Received: March 9, 1999*

Pulsed field gradient nuclear magnetic resonance has been successfully applied to a direct and detailed experimental study of topological and dynamic aspects involved in the exchange of small, nonsorbed fluid molecules between the intraparticle pore network and the interparticle void space in chromatographic columns packed with spherical-shaped, porous particles. The approach provides quantitative data about the effective, intraparticle diffusion coefficients (and tortuosity factors) and about the associated, diffusion-limited mass transfer kinetics, including stagnant boundary layer contributions. In view of the recorded exchange kinetics, an analytical description for solute diffusion into/out of spherical particles is offered and addresses the influence of the particle size distribution and particle shape on the observed mass transfer rates and calculated diffusivities. The combined analyses of the steady-state intraparticle pore diffusion data and the associated exchange kinetics with Peclet numbers up to 500 reveals the existence of external stagnant fluid where all the interparticle fluid-side resistance to diffusion is localized. It is represented by a thin stagnant boundary layer around the particles and can be accounted for by the introduction of a hydrodynamically effective particle diameter which is found to depend on the Peclet number. The approach appears to be promising for a selective, detailed study of the boundary layer dynamics. Concerning the investigation of different chromatographic media and intraparticle morphologies, we demonstrate that the actual correlation (or randomness) of interconnection between intraparticle pores of different size has a profound effect on the observed tortuosity factors and the diffusion-limited stagnant mobile phase mass transfer kinetics. Compared to intraparticle pore networks with a random assignment of different pore sizes, hierarchically structured bidisperse porous particles offer a superior network topology, which can form the basis for an increased chromatographic performance.

## Introduction

The packed and consolidated bed of a chromatographic column obtained with spherical-shaped, porous, rigid particles intrinsically bears a complex fluid dynamics. It is difficult to analyze exactly, due not least to the number of different mechanisms that actually contribute to the dispersion of a solute band as it passes through the column and to the complex geometries of the intraparticle pore network and the interparticle void space involved in this tortuous journey.[1−3] Under typical conditions, solute transport occurs mainly by interparticle convection and intraparticle diffusion, and chromatographic separations are generally achieved by a differential adsorption of the solutes on the large inner surface area of the packing materials. The adsorption process requires that solute first moves through a film of fluid at the outer surface of the adsorbent particles (most often assumed to be stagnant), where diffusion normal to the surface is at least the dominating transport mechanism,[4−7] and then diffuses through the pools of stagnant fluid entrained in the intraparticle pore network.[8−13] In most practical cases, the adsorption−desorption process is fast and the equilibrium kinetics are controlled by the mass transfer resistances. In this respect, the stagnant mobile phase mass transfer, i.e., the diffusion of solute molecules into and out of the fine pores of the particles, has been identified as the major source of band dispersion in liquid chromatography.[1,14−16] Especially with smaller partition coefficients of the solute and a larger particle radius, this diffusion-limited mass transfer within the particles may dramatically limit the overall kinetics.[9]

Advances in the design and preparation of adsorbents have included the use of small nonporous[17,18] and micropellicular particles,[19] continuous polymer phases[20] and monolithic structures[21] as an alternative to packed beds, as well as the development of hierarchically structured, macroporous[22] and gigaporous particles (with $d_{pore}/d_p > 10^{-2}$).[23,24] In the case of the latter, intraparticle fluid forced convection has been proposed to be operative under certain conditions, to assist and even dominate over the diffusive transport in the larger, particle-transecting ("flow-through") pores of the bidisperse pore network inside these particles.[25−28] Because of the higher mass transfer rates columns packed with these gigaporous media have shown significant performance advantages over columns obtained with conventional, purely diffusive adsorbent particles, especially in high-speed separations and purifications of slowly diffusing (bio)macromolecules.

Central to the understanding of a diffusion-controlled mass transfer kinetics in porous particles and to the prediction of the chromatographic performance of a material is the effective diffusivity ($D_{eff}$) of and in the stagnant fluid entrained in the intraparticle pore network. This parameter inherently contains a wealth of information and in the general case is related to the bulk diffusivity in free solution ($D_m$) by[29,30]

$$\frac{D_{eff}}{\epsilon_{intra}} = \frac{D_m}{\tau_{intra}} \frac{K_p}{K_H} \tag{1}$$

* To whom correspondence should be addressed. Phone: + 31 (317) 48-2047. Fax: + 31 (317) 48-2725. E-mail: ulrich.tallarek@water.mf.wau.nl.

10.1021/jp990828b CCC: $18.00 
Published on Web 08/21/1999

with $\epsilon_{intra}$, the internal porosity of the particles and $\tau_{intra}$, the tortuosity (more correctly,[31] the tortuosity factor) of the intraparticle pore network. The enhanced drag coefficient, $K_H^{-1}$, is a factor accounting for additional hydrodynamic hindrance within the pore when solute and pore size are of comparable magnitudes. $K_P$ is the partition coefficient and characterizes the ratio of solute concentration inside the pores to the concentration outside the pores in bulk solution at equilibrium. This entropy-controlled, geometric exclusion effect is intimately related to the basic retention mechanism in gel permeation chromatography.[32,33] The restrictive factor $F_\lambda = K_P/K_H$ is a function dependent on $\lambda$, the ratio of the critical molecular diameter to the pore diameter, and ranges between 0 and 1.[30]

For diffusion-limited mass transfer kinetics and small values of $\lambda$ ($F_\lambda \approx 1$) the effective diffusivity remains the ultimate transport parameter relating—commonly expressed by a single tortuosity factor (and the respective network porosity)—diffusive flux into and out of the particles pores to the intrinsic system morphology (geometry and topology) and range of inhomogeneities. It includes surface characteristics (e.g., chemical modification and roughness), the pore size and its distribution(s), pore shape, and pore interconnectivity. For a network made of cylindrical pore segments the effective diffusivity may be expressed by[34,35]

$$D_{eff} = \frac{1}{\tau_{intra}} \int_{\mathbf{r}} D(\mathbf{r}) \cdot \epsilon_{intra}(\mathbf{r})\, d\mathbf{r} \qquad (2)$$

where $\epsilon_{intra}(\mathbf{r})d\mathbf{r}$ stands for the porosity of pores having a radius in the interval $[\mathbf{r}, \mathbf{r} + d\mathbf{r}]$, and $\epsilon_{intra}(\mathbf{r})$ is the porosity density function which may account for the length and size distribution of the (cylindrical) pores.[35] Unfortunately, this equation does not contain much information about the actual correlation of the interconnection between pores of different size that contribute to $\epsilon_{intra}(\mathbf{r})$, an effect that certainly has a strong influence on the network permeability and value of $\tau_{intra}$. The tortuosity factor is a very sensitive indicator for the presence of dead-end pores which adversely affect stagnant mobile phase mass transfer rates[36−38] and may cause excessive bandbroadening and peak tailing.[39,40] At a given porosity and pore size distribution the tortuosity is lower for pore networks with higher coordination numbers.[41,42]

Closely related to the effective diffusivity is the intraparticle diffusivity $D_{intra}$, but compared to $D_{eff}$ it is based on the pore-level solute concentration and consequently does not account for the porosity factor and the equilibrium partition coefficient[43]

$$D_{intra} = \frac{D_m}{\tau_{intra}} \frac{1}{K_H} \qquad (3)$$

Thus, the problem now is to predict the values of the intraparticle tortuosity factor, $\tau_{intra}$ (for $K_H^{-1} \approx 1$). Finally, although with silica it is reasonable to assume that no mass transfer can take place through the walls between pores, this is not necessarily true for all the resins used as packing materials.[44] For this diffusion in and through the polymer matrix itself, the diffusion coefficient would be unusually small, causing low intraparticle sorption rates.[45,46] Although estimation procedures are available, it still remains very complicated to make accurate predictions of the diffusivities and tortuosities needed for liquid chromatography and bioreactor modeling, including diffusion and reaction in porous catalysts.[47] Despite its importance and historical background,[1,2] the direct and quantitative measurement of the classical stagnant (i.e., diffusion-limited) mobile phase mass transfer kinetics also has been extremely difficult.

Based on the averaged propagator formalism for nuclear spin (hence, molecular) displacements, pulsed field gradient nuclear magnetic resonance (PFG-NMR) is currently attracting increased interest—by choice acting as a contrast mechanism in an NMR imaging approach—in the experimental characterization of fluid flow and dispersion within a number of porous model systems.[48−56] This includes specific packed-bed applications in high performance liquid chromatography and heterogeneous catalysis, such as the study of axial and transverse plate height relations in analytical columns[57] or the performance of preparative-scale, radially compressed cartridges,[58] and effective diffusivity measurements in porous catalyst pellets.[59] In particular, it has been demonstrated most recently that this approach allows to observe directly, separately and quantitatively the purely diffusive, intraparticle and the diffusive-convective interparticle fluid molecules in chromatographic columns packed with porous adsorbent particles.[60]

In this article we report about an extended, detailed PFG-NMR investigation of the stagnant mobile phase mass transfer kinetics and intraparticle diffusivities of several single-fluid phases in selected chromatographic media. Special attention is given to the influence of structural parameters, such as the particle size and (intraparticle) pore size distributions, and to the actual correlation of interconnectivity between, e.g., large and small pores on the observed intraparticle fluid transport characteristics, such as the tortuosity factor and the rates of fluid exchange with the interparticle void space. It is demonstrated that this potential PFG-NMR approach provides important, in fact complementary data of both steady-state and transient nature concerning intraparticle diffusion and the associated, diffusion-limited mass transfer kinetics. The combined use of these series of data allows an unambiguous determination of intraparticle diffusivities and tortuosity factors and of the contribution to the observed mass transfer characteristics at a given Peclet number of stagnant regions in the interstitial space of packed beds, i.e., of those between and around the fine particles. The obtained results are compared to dimensional considerations concerning the stagnant boundary layer and its hydrodynamics available from literature data.

## Experimental and Procedural Section

The 4.6 × 150 mm poly(arylether-ether-ketone) columns were professionally packed and consolidated using the slurry technique (Grom Analytik + HPLC GmbH, Herrenberg, Germany),[61,62] following the detailed instructions of the respective manufacturer. The PEEK material allows the columns to be packed and operated at pressures up to 350 bar and also shows an excellent magnetic susceptibility characteristics.[63] $^1$H PFG-NMR measurements were made at 23 ± 0.5 °C on a 0.5 T NMR spectrometer. A more detailed description of the NMR hardware configuration and the liquid chromatography implementation can be found in a previous article.[54] Solvents were of LiChrosolv quality (Merck, Darmstadt, Germany) and degassed with helium before use.

Some characteristics of the packing materials used in this work are listed in Table 1. Particle characterization (mean diameter and standard deviation of particle size distribution) was performed by laser light scattering on a Coulter LS 130 particle size analyzer (Beckman Coulter, Inc., Fullerton, CA). Two of these supports are based on a polystyrene (PS) matrix cross-linked with divinylbenzene (DVB). One is a so-called perfusive support with a rather bimodal intraparticle pore network, which in this case is due to the hierarchical design of these particles (POROS 50 R2 from PerSeptive Biosystems,

**TABLE 1: Some Characteristics of the Spherical-Shaped, Rigid Porous Particles**

| properties: material | YMC ODS-A S50 | POROS 50 R2 | SOURCE 30Q |
|---|---|---|---|
| mean diameter, $d_p$ [$\mu$m] | 50.2 | 49.6 | 30.7 |
| standard deviation [$\mu$m] | 10.6 | 9.5 | 0.7 ($<0.03d_p$) |
| matrix | C18-bonded silica, fully endcapped | cross-linked PS-DVB, hierarchically structured | cross-linked PS-DVB, quaternary ammonium |
| internal porosity[a] | | $\sim 0.5$ | |
| average pore sizes [Å] | $120 \pm 15$, unimodal distribution | 6000−8000, 500−1500; bimodal distribution | 200−10000, unimodal distribution |

[a] According to the information provided by the respective manufacturer.

Wiesbaden, Germany).[23,64] The second consists of extremely monodisperse spheres, which is due to the salient features of the Ugelstad method[65] on which the particles are based, with a comparatively broad, unimodal intraparticle pore size distribution (SOURCE 30Q from Amersham Pharmacia Biotech, Freiburg, Germany). These monosized beads are substituted with quaternary ammonium groups which are attached to the matrix via long, hydrophilic spacer arms (strong anion exchanger). In addition to the two PS-DVB supports we used conventional reversed-phase particles based on a porous silica matrix (YMC•GEL ODS-A S50 from YMC Europe, Schermbeck, Germany).

For an ideal PFG-NMR experiment[66] and in the absence of any spatial localization gradients the normalized echo amplitude, $E(\mathbf{q},\Delta)$, bears a direct Fourier relation with the Lagrangian averaged propagator, $\bar{P}(\mathbf{R},\Delta)$, of the fluid molecules[67−69]

$$E(\mathbf{q},\Delta) = \frac{S(\mathbf{q},\Delta)}{S(0,\Delta)} = \int_{\mathbf{R}} \bar{P}(\mathbf{R},\Delta)\exp(i2\pi\mathbf{q}\cdot\mathbf{R})\, d\mathbf{R} \qquad (4)$$

The displacement probability distribution $\bar{P}(\mathbf{R},\Delta)$ gives the probability for any fluid molecule in the sample to travel a net displacement, $\mathbf{R}$, over time $\Delta$ in the direction of the applied pulsed magnetic field gradients of amplitude $|\mathbf{g}|$ and duration $\delta$.[69] This gradient area defines the vector $\mathbf{q} = (2\pi)^{-1}\gamma\delta\mathbf{g}$ in $\mathbf{q}$-space, which is the space reciprocal to the dynamic displacement $\mathbf{R}$.[70−72] Thus, $\bar{P}(\mathbf{R},\Delta)$ can be reconstructed directly from the PFG-NMR signal by Fourier transform of $E(\mathbf{q},\Delta)$ with respect to $\mathbf{q}$. When on the observational time scale both the intraparticle diffusion and the convection-driven interparticle dispersion processes of the fluid molecules are Gaussian in nature,[54] the net amplitude attenuation of $E(\mathbf{q},\Delta)$ as a function of $\mathbf{q}$ is modulated, as long as the exchange between stagnant intraparticle and moving interparticle fluid is still incomplete over time $\Delta$, by the respective two (also Gaussian) decay envelopes representing the intraparticle diffusivity $D_{intra}$ and the apparent axial dispersion coefficient $D_{ap,a}$. Including in general the possibility of differences in the longitudinal ($T_1$) and transverse ($T_2$) relaxation time characteristics of the fluid molecules in the intra- and interparticle pore space environments,[73,74] we then obtain for $S(\mathbf{q},\Delta)$[68]

$$S(\mathbf{q},\Delta) = \sum_{n=1}^{2} A_n(\Delta)\exp\left[-4\pi^2\mathbf{q}^2 D_n\left(\Delta - \frac{\delta}{3}\right) - \frac{(\kappa_2 - \kappa_1)}{T_{1,n}} - \frac{2\kappa_1}{T_{2,n}}\right] \qquad (5)$$

Here, $\kappa_1$ and $\kappa_2$ denote the time of the (nonselective) second and third 90° r.f. pulse in the pulsed field gradient stimulated echo sequence used in this work.[75,76] On the basis of the dynamic displacements $\mathbf{R}$ over time $\Delta$, the $A_n(\Delta)$ in this case represent the number of fluid molecules which have remained in stagnant regions of the packed bed or which have (at least once) participated in the interparticle flow, respectively. Experiments at different observation times $\Delta$ ($\kappa_2$ varied) were generally performed with a constant gradient pulse duration ($\delta = 2.5$ ms and $\delta \ll \Delta$) but incremented gradient amplitude, taking 64 $\mathbf{q}$-steps in the range of $\pm\mathbf{q}_{max}$ and up to 48 phase-alternated signal averages at each value of $\mathbf{q}$. By keeping $\kappa_1$ fixed, the contribution of transverse relaxation in eq 5 is also constant. Echoes were acquired on-resonance and were phased individually to extract the net amplitude modulation of $S(\mathbf{q},\Delta)$ at a given flow rate and observation time. For the calculation of $D_{intra}$ and $A_{intra}(\Delta)$ individual measurements were repeated at least three times, with $r^2 > 0.9996$ for the best fit of the raw data to eq 5 and a reproducibility of the results within 5%.

All calculations were performed using IDL (Interactive Data Language, Research Systems Inc., Boulder, CO). To account for the contribution of intraparticle longitudinal relaxation over time $(\kappa_2 - \kappa_1) = (\Delta - \kappa_1)$ to the slope of the $A_{intra}(\Delta)$ vs $\Delta$ curve (cf. Equation 5), combined $T_1/T_2$ $^1$H relaxation time measurements were made with a standard inversion−recovery technique ($T_1$), incorporating a proper echo-train ($T_2$). These measurements did not reveal the existence of discrete $T_1$ distributions for the intraparticle and the interparticle fluid molecules. Although the surface-to-volume ratios of the respective pore spaces are different, it suggests that surface relaxation is not strong enough to impart a significant difference in longitudinal relaxation behavior. It is probably caused by the low-field NMR measurements ($^1$H 20.35 MHz), combined with the extremely low amount of paramagnetic impurities present in these chromatographic media and the respective chemical modification of the particles (internal and external) surfaces. In the case of the porous silica particles (the only inorganic oxide-based particles used in this work), for example, the $Fe^{3+}$ contamination of the parent silica is well below 10 ppm. From a chromatographic point of view, surface trace metal impurities would give strong Lewis acid adsorption sites which adversely affect performance.[77] Further, the originally polar, silanolic surface has been chemically derivatized by a bonded alkyl layer (high coverage of $C_{18}$ chains), including a $C_1$-endcapping of residual silanols. It is a classical chromatographic support used for many reversed-phase separations, most applicable for polar to moderately nonpolar samples. Thus, returning to the NMR standpoint, surface (and bulk) trace metal activity is very small, and the respective sites become sterically almost inaccessible.

## Results and Discussion

With respect to the actual fluid dynamics encountered in the experiments, Figure 1a shows a representative single-fluid phase averaged propagator distribution, $\bar{P}(\mathbf{R},\Delta)$, recorded in the axial (flow) direction, at a volumetric flow rate ($F_v$) of 8.0 mL/min and an observation time ($\Delta$) of 25 ms. This quantitative displacement probability distribution illustrates both the potential steady-state character (regarding intraparticle diffusion) and transient nature (with respect to the stagnant mobile phase mass transfer kinetics) of these PFG-NMR measurements. For

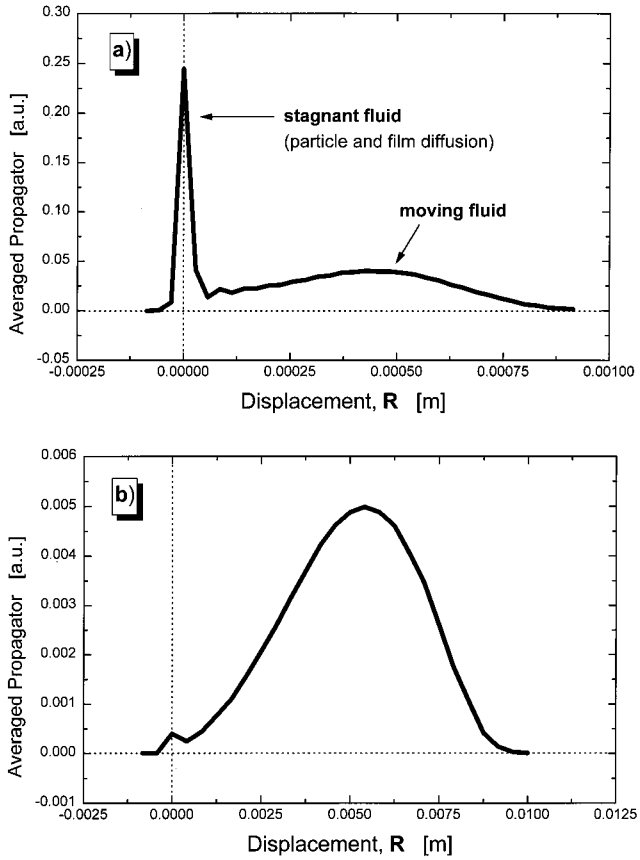


**Figure 1.** Axial displacement probability distributions of the fluid molecules (water) in a packed bed of porous particles (YMC ODS-A S50). 4.6 × 150 mm PEEK column; volumetric flow rate $F_v$ of 8.0 mL/min. The stagnant, purely diffusive fluid is found centered at zero net displacement. Observation times, $\Delta = 25$ ms and $\Delta = 420$ ms.

example, under the experimental conditions (Figure 1a), we find 24.6% of the water molecules in the packed bed being left unexchanged in the deep stagnant pools inside the porous C18 silica particles. By a systematic variation of the observation time, this actually transient character of the measurement allows to record the stagnant mobile phase mass transfer kinetics toward a complete exchange between stagnant and moving fluid in the packed bed.[54] As is demonstrated in Figure 1b, at $\Delta = 420$ ms only less than 0.5% of the stagnant water remains unexchanged. On the basis of tortuosity factor, the average size and spherical shape of the particles it should be finished after some characteristic exchange time, $\Delta_e$, assuming that the fluid molecules have to travel a net distance of $d_p/2$ (from the spheres center to its external surface) to leave the porous particles completely[1]

$$\Delta_e = \frac{\tau_{intra}}{2\,D_m}\left[\frac{d_p}{2}\right]^2 \qquad \text{with} \qquad (\sqrt{\langle \mathbf{R}^2_{intra}\rangle})_{\Delta=\Delta_e} = \frac{d_p}{2} \quad (6)$$

We will see how this dimensional consideration matches the experimental data. On the other hand, the root-mean-squared (rms) translational displacement of the yet unexchanged intraparticle fluid molecules (as long as $\Delta < \Delta_e$, cf. Figure 1a) probed in the direction of the applied magnetic field gradient is given by

$$\sqrt{\langle \mathbf{R}^2_{intra}\rangle} = (2\,D_{intra}\Delta)^{1/2} \quad (7)$$

For the particle dimensions of the chromatographic media, mobile phase diffusivities and observation times selected for this study, the corresponding diffusive displacements of the

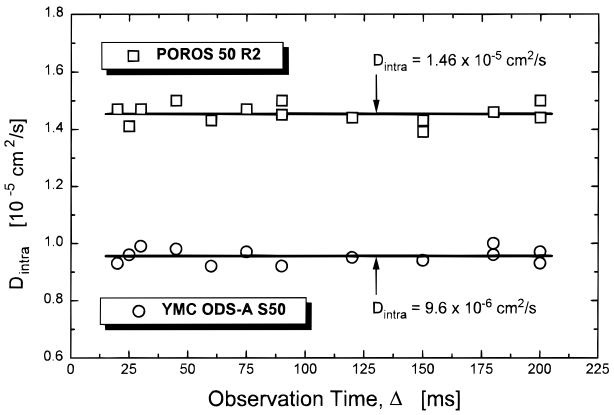


**Figure 2.** Intraparticle self-diffusion coefficient of water in two of the chromatographic media as a function of the observation (diffusion) time; $F_v = 8.0$ mL/min.

stagnant fluid molecules are much larger than the range of typical inhomogeneities in either intraparticle pore network. In this respect, the experiment then provides a steady-state pore diffusion measurement which allows to extract an effective intraparticle diffusion coefficient, $D_{intra}$. Furthermore, these data necessarily have to be consistent with the characteristic decay rates of the aforementioned, diffusion-limited exchange kinetics. These two series of data in fact provide us with complementary information, not only in view of the stagnant (diffusion-controlled) boundary layer existing at the particles external surface under laminar flow conditions.[5] Consequently, the obtained results are now discussed separately under the light of these aspects.

**Intraparticle, Effective Self-Diffusion Coefficients.** The single fluid phases used in this study consist of water, acetonitrile, methanol, 2-propanol, and methylene chloride. These nonsorbed molecules are rather small compared to the pore constrictions encountered inside the porous particles. Thus, hydrodynamic friction is negligible and the directly measured intraparticle rms translational displacements (and $D_{intra}$) at long enough times approach the values given by the topology, i.e., the interconnectiveness of the pore network, by means of eq 3 (with $K_H^{-1} \approx 1$). Because only single-fluid phases are used, the calculated values of $D_{intra}$ represent the corresponding self-diffusion coefficients.[78]

Because of different mean pore sizes, pore size distributions, and pore interconnectivities in the particles (Table 1), the associated transport heterogeneities in the respective pore networks are expected to be characterized by different correlation times and length scales. Figure 2, however, demonstrates that, within the range of observation times $\Delta$ encountered in the measurements, $D_{intra}$ in fact is found independent of this parameter and in the tortuosity-limited regime of the respective pore network, corresponding to a steady-state pore diffusion in either case (i.e., such that $D_{intra} \equiv D^{eff}_{intra} = D_m/\tau_{intra}$). Otherwise, $D_{intra}$ would depend on $\Delta$ and still decrease toward the tortuosity asymptote. The attainment of a steady-state pore diffusion, together with its verification here by the data shown in Figure 2 is also important with respect to the average particle diameters (Table 1). For example, when larger pores start to contribute to the intraparticle porosity, the pore network becomes inhomogeneous on an increasing scale that may approach the size of the whole particle. On the other hand, as long as the asymptotic (tortuosity limited) diffusion regime is reached, the tortuosity factor of a network consisting of 100% small pores is the same as with 100% large pores.[42]

**TABLE 2: Intraparticle Tortuosity Factors, $\tau_{intra} = D_m/D_{intra}$**

| fluid: material | YMC ODS-A S50 | POROS 50 R2 | SOURCE 30Q | $D_m$ [$10^{-5}$ cm$^2$/s] |
|---|---|---|---|---|
| water | 2.24 | 1.47 | 2.08 | 2.15 |
| acetonitrile | 2.29 | 1.56 | 2.16 | 3.83 |
| methanol | 2.23 | 1.51 | 2.11 | 2.23 |
| 2-propanol | 2.15 | 1.43 | 2.03 | 0.58 |
| methylenechloride | 2.21 | 1.53 | 2.09 | 3.07 |

The intraparticle tortuosities measured by PFG-NMR are summarized in Table 2, and the discussion necessarily focuses on the topology of the three pore networks. The most striking feature of these data is the tortuosity factor of the gigaporous particles (POROS 50 R2) which, for all the mobile phases considered in this work, is significantly lower than that of the other two supports. In contrast to conventional media, these POROS beads have two discrete classes of pores interconnected in a well-correlated manner.[23] The bidisperse particles are made by inter-adhering PS-DVB microspheres which are fused into the final, continuous particle structure by using several steps of clustering. This process creates a first set of 6000−8000 Å pores which transect the whole particle (throughpores) and a second, more abundant set of smaller pores with 500−1500 Å in diameter. Because of the hierarchical design of these particles, the spacing between throughpores is seldom greater than 1 $\mu$m, thereby reducing diffusion path lengths in the interconnecting smaller pores to below that distance.[23] Thus, the actual correlation of interconnectivity between the large and small pores creates a gigapore network ($d_{pore}/d_p > 10^{-2}$) that spans the whole particle and minimizes diffusion distances in the macroporous domain ($d_{pore} > 500$ Å). On the basis of the lower network tortuosities, the stagnant mobile phase mass transfer rates within such hierarchical bidisperse networks will be superior compared to bidisperse structures in which the pore sizes are assigned at random.[79,80] The transport behavior of such nonrandom bidisperse pore networks in fact is expected to be closer to that of the individual giga- and macropore (or macro- and mesopore) networks arrayed in parallel rather than to the behavior of the corresponding random network with bimodal pore size distribution.[81] Although the correlation of interconnectivity is now well-recognized as being of prime importance in the design of (bidisperse) porous particles,[79−83] surprisingly little experimental data (like $D_{intra}$) are available which directly characterize the topology of these hierarchically structured pore networks compared to less correlated ones.

In contrast to the 50-$\mu$m PS-DVB particles (POROS 50 R2), the pore network of the 30-$\mu$m beads (SOURCE 30Q) is characterized by a relatively broad, unimodal pore size distribution, with the interconnection of the larger and smaller pores being rather uncorrelated, i.e., comparatively random. Thus, the large and small pores do not form interconnected, distinct pore networks, and the tortuosity factor then increases due to the shielding of large pores by small ones (Table 2).[84] Finally, the yet slightly higher intraparticle tortuosity factors found for the mesoporous silica-based particles (YMC ODS-A S-50) could be caused by the presence of a larger number of dead-end pores. However, the exact topological differences of the latter two pore networks are hardly known with sufficient accuracy to allow such small distinctions to be made meaningfully. Nevertheless and as a more general trend in view of the arguments followed in this work, the tortuosity factors observed for the nonhierarchical intraparticle pore networks are significantly higher than those found for the hierarchical bidisperse particles; however, the values are still close to 2. This value has been predicted for an isotropic porous medium,[31] recalling the basic arguments of Carman[85] in context of the parallel-pore model. Other arguments suggest a tortuosity factor of 3 for a particle network consisting of randomly oriented, nonintersecting cylindrical pores where each straight capillary covers the length of the whole particle.[86]

**TABLE 3: Cubic Lattices of Identical Spheres at Dense Packing**

| cubic lattice | coordination number | interstitial porosity | tortuosity factor |
|---|---|---|---|
| SC | 6 | 0.476 | 1.38 |
| BCC | 8 | 0.320 | 1.47 |
| FCC | 12 | 0.259 | 1.62 |

With respect to the remarkably lower value of $\tau_{intra}$, the hierarchical bidisperse particles can be viewed as consisting of loosely packed agglomerates being responsible for the several types of pores finally present in the matrix.[23] Thus, the actual network within a single support particle resembles itself, to some degree at least, the overall (intra- and interparticulate) pore space typically encountered in packed beds of porous particles. Using this similarity for a moment, Table 3 summarizes some properties of cubic, i.e., regular lattices of identical, impenetrable spheres at dense packing so that the hard spheres are just touching each other.[87,88] An increase in the distance between neighboring spheres (or corresponding decrease, while spheres start to overlap) causes also an increase (decrease) in the interstitial porosity and in the effective, translational diffusivity of small molecules entrained in the respective pore network.[89] Further, any kind of positional disorder introduced into the particle arrangement (at a constant porosity) leads to an increased lengthscale of heterogeneities and a higher tortuosity factor.

Given the fact that a conservative estimate for the intraparticle porosity of the hierarchically structured particles (POROS 50 R2) is 0.5,[23] comparison with Table 3 and the tortuosity factors given in Table 2 suggests that neither regular (cubic) lattice at dense packing is appropriate to describe well this pore network. On the basis of a pure value identification, the simple cubic arrangement comes closest. Not surprisingly, it is the one with the smallest coordination number. These observations are in agreement with recent findings that the pore structure of these particles rather behaves like an inhomogeneous assemblage of loosely packed microspheres.[90] This situation is quite different from the one typically encountered in random close-packed beds of chromatographic columns. Here, the interparticle porosity is usually found to vary between 0.36 and 0.4. More extreme values are possible, depending on packing and operational procedures, as well as on particle characteristics.[91]

Remarkably low intraparticle tortuosity factors have also been postulated for hierarchically structured, spherical, porous zirconia particles using PFG-NMR methods.[92,93] Even though the authors did not report the net effective, intraparticle diffusion coefficients, the trend in their diffusivity data at least indicates values of $\tau_{intra}$ between 1.5 and 2 (i.e., below the isotropic porous medium value). This behavior has been attributed to the very open packing of the colloids within the particles.[92] Higher tortuosity factors, yet close to 2, have been reported for protein diffusion within macroporous size-exclusion chromatographic media.[43,94] By restricting the diffusing species to individual

particles using excluding solvent in the interparticle void space, intraparticle labeled-protein (tracer) diffusion could be studied selectively by fluorine PFG-NMR.

All these data seem to indicate a general trend for the actual hierarchy in pore structure and the associated tortuosity factor. However, they also call for further studies demonstrating systematically its dependence on the processing conditions and thereby achieved correlation (or randomness) of interconnection between differently sized pores. These experimental data will help in the refinement of chromatographic separations[95] and in the development of a numerical approach (and model validation in general) for predicting the interrelationship of structure and transport in porous adsorbent particles.[96]

Another aspect closely related to the intraparticle diffusivity of the hierarchically structured particles (POROS 50 R2) merits attention. On the basis of dimensional considerations and morphological observations concerning the gigaporous (through-pore) network, it has been proposed that these hierarchically bidisperse particles can be operated under perfusion conditions, i.e., in such a mode that both intraparticle forced-convection and diffusion contribute to the fluid transport in the gigapores, while only diffusion is active in the smaller macropores.[23] According to Liapis and McCoy,[97] the term "perfusion chromatography" refers to any chromatographic system in which the intraparticle fluid velocity is nonzero. The effect of intraparticle convection is an enhancement of the overall rate of mass transfer in the particle, thereby improving the efficiency of diffusion-limited chromatographic operations. It has been pointed out conceptually that its contribution can be well-represented by a convection-augmented effective, intraparticle diffusivity.[23,98] The first experimental direct confirmation of net flow through gigaporous particles has been reported recently in a test apparatus that isolates single particles.[90] Figure 3a however shows that within the range of hydrodynamic conditions encountered in our current work, $D_{intra}$ in all the chromatographic media remains constant in the purely diffusive, tortuosity-limited regime ($D_{intra} < D_m$ and $\tau_{intra} > 1$). As can be concluded from Figure 3b which records the accompanying pressure drop over the 4.6 × 150 mm columns and also from a comparison with the results reported by Pfeiffer et al.,[90] the actual pressure gradient across individual particles in the packed bed is probably too small to act as a driving force for any measurable intraparticle forced-convection assisting or even dominating fluid transport. Thus, compared to the other two supports, the low tortuosity factor recorded for the hierarchically bidisperse particle structure resembles diffusion control in a yet superior pore network, without the need to postulate, at this stage at least, the operation of a perfusive mechanism.

Next, we turn to the stagnant mobile phase mass transfer kinetics which is associated with the exchange of fluid molecules between the investigated purely diffusive intraparticle pore network (already with a preknowledge of the respective values of $D_{intra}$) and the diffusive-convective interparticle void space, how we can acquire and analytically describe it, and to the complementary information it provides.

**Nonsteady-State Diffusion into/out of Spherical Particles.** On the basis of the net (dynamic) displacements of the fluid molecules over time Δ, the propagator formalism provides a quantitative characterization of the stagnant and moving fluid in the packed bed using the PFG-NMR technique. Averaged propagator distributions recorded at increasing observation times thus directly monitor the progressive diffusion out of the spherical particles.[60] Those fluid molecules which leave the spheres and participate in the interparticle forced convection

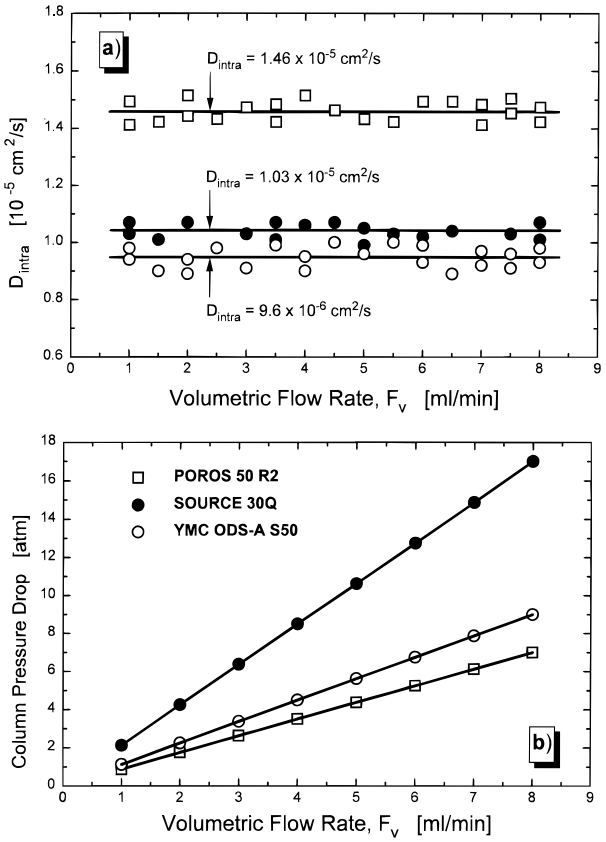


**Figure 3.** Intraparticle self-diffusion coefficients of water in (a) the chromatographic media and (b) column pressure drop as a function of the volumetric flow rate; Δ = 60 ms.

within (increased) time Δ will no longer contribute to the ensemble of purely diffusive fluid molecules which is found centered at zero net displacement. At long enough observation times the stagnant fluid fraction has disappeared and exchange is complete (cf. Figure 1). Consequently, this situation resembles the general case of an unsteady-state diffusion of a solute into/out of spherical, porous particles in which the spheres are emptied or, vice versa, filled by diffusion, and it can be treated analytically in the same manner. Thus, when we then consider the case in which the diffusion (no chemical reaction yet) from the bulk of the particle of radius $r_p$ to its surface is radial, i.e., the initial and surface conditions are such that the concentration $C$ of a solute only depends on $r$ and time Δ, the diffusion equation for a constant diffusion coefficient takes the form[99]

$$\frac{\partial C}{\partial \Delta} = D_{intra}\left[\frac{\partial^2 C}{\partial r^2} + \frac{2}{r}\frac{\partial C}{\partial r}\right] \tag{8}$$

With the substitution $u = Cr$ and assuming an initial concentration $C_i(r)$ in the sphere and surface concentration $C_s(\Delta)$, the equations for u become[99]

$$\frac{\partial u}{\partial \Delta} = D_{intra}\frac{\partial^2 u}{\partial r^2} \qquad \text{for} \qquad 0 \le r < r_p \tag{9}$$

with

$u = 0$ when $r = 0$ and $\Delta > 0$

$u = C_s(\Delta)\cdot r_p$ when $r = r_p$ and $\Delta > 0$

$u = C_i(r)\cdot r$ when $0 \le r < r_p$ and $\Delta = 0$

These are the equations for diffusion in a slab of thickness $r_p$, with its ends at $r = 0$ and $r = r_p$ kept at zero and $C_s(\Delta)r_p$ respectively, and with the initial distribution $C_i(r)r$. Thus, the problem of radial diffusion in (uniform) spheres can be deduced from the solution of the corresponding linear problem. Equation 9 is of the same form as the analogous differential equation characterizing heat transfer for unsteady-state heat conduction in plane sheets (and spheres). For that case, Carslaw and Jaeger[100] have derived an analytical solution which is the product of a trigonometric and an exponential series. In terms of the differential equation (eq 9) and the boundary conditions that the sphere initially is at a uniform concentration ($C_i(r)$ = constant = $C_0$) and that the concentration at the surface of the sphere is maintained steady at zero ($C_s(\Delta)$ = constant = 0), which causes the sphere to be emptied by diffusion, the average amount of diffusing substance still remaining in the sphere at any time, $A_{intra}(\Delta)$, is given by[100]

$$\frac{A_{intra}(\Delta)}{A_{intra}(0)} = \frac{6}{\pi^2}\sum_{n=1}^{\infty}\frac{1}{n^2}\exp\left[-n^2\pi^2\frac{D_{intra}\Delta}{r_p^2}\right] \qquad (10)$$

The corresponding solution for small exchange times (and small values of the dimensionless parameter $\zeta = (D_{intra}\Delta/r_p^2)$ is

$$\frac{A_{intra}(\Delta)}{A_{intra}(0)} = 1-6\left[\frac{D_{intra}\Delta}{\pi r_p^2}\right]^{1/2} + \frac{3D_{intra}\Delta}{r_p^2} - 12\left[\frac{D_{intra}\Delta}{r_p^2}\right]^{1/2}\sum_{n=1}^{\infty}\text{ierfc}\frac{nr_p}{\sqrt{D_{intra}\Delta}} \cong 1-6\left[\frac{\zeta}{\pi}\right]^{1/2} + 3\zeta \qquad (11)$$

At large observation (exchange) times $\Delta$, on the other hand, eq 10 approximates to a simple exponential decay function

$$\frac{A_{intra}(\Delta)}{A_{intra}(0)} = \frac{6}{\pi^2}\exp[-\pi^2\zeta] \qquad (12)$$

Figure 4a shows the dependence on the observation time of the amount of stagnant water entrained in the respective particle packings. At first glance, all the mass transfer data are well-described by eq 10 and values of the constant $B = D_{intra}\pi^2/r_p^2$ obtained from the best fit of the data to this equation are summarized in Table 4, together with the corresponding values obtained by use of eqs 11 and 12 at short and long times, respectively. Evidently, the experimental approach followed in this work using single-fluid phases, while monitoring a (fictitious) diffusional emptying of the porous particles (Figure 4a), avoids problems that could arise due to a nonconstant (i.e., concentration-dependent) diffusion coefficient during transient diffusion experiments.[101]

A closer look at the data however reveals slight, but characteristic deviations from the best fit to eq 10 which inherently assumes, apart from a constant diffusion coefficient, a uniform diameter of the spherical particles. In this respect, both the particle shape and a size distribution will have a pronounced effect on the experimental mass transfer curves.[102] Compared to the predictions of eq 10, smaller-than-average particles will cause a higher initial rate, while the larger-than-average particles will be responsible for lower decay rates at long times, especially when $A_{intra}(\Delta)/A_{intra}(0)$ becomes smaller than about 0.2. This is exactly what we observed for the supports with the larger particle size distribution (Figure 4b and Table 4). In view of the fact that the monodisperse polymer particles (SOURCE 30 Q) have a remarkably narrower particle size distribution than the other two supports (cf. Table 1),[65] the effect was investigated further. In passing we note that the influence of the particle shape is not addressed separately and that a perfect spherical shape of the particles is assumed, a fairly reasonable assumption for these modern supports as can be shown by electron microscopy of the media.

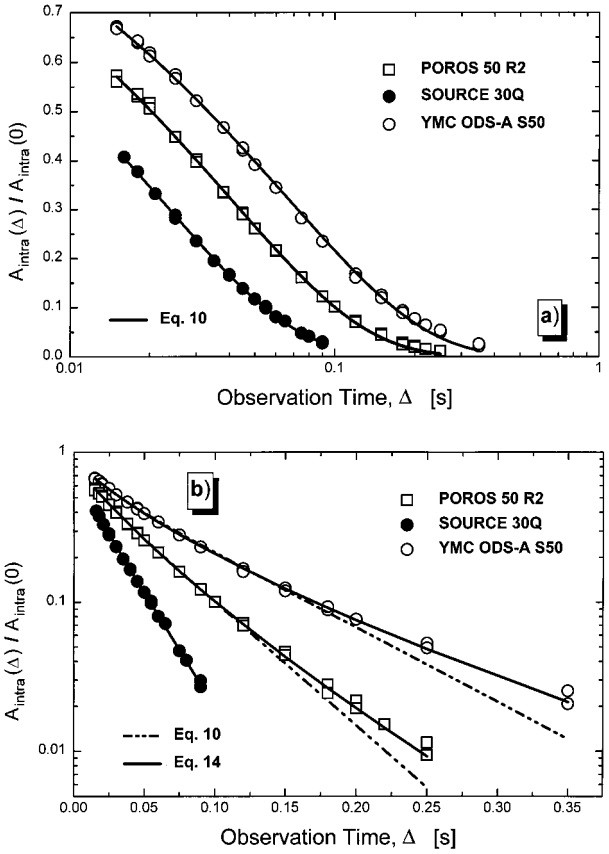


**Figure 4.** (a) Unsteady-state diffusion and total intraparticle fluid fraction unremoved as a function of the observation time. Mobile phase, pure water. $F_v$ = 4.8 mL/min (30 $\mu$m particles) and 8.0 mL/min (50 $\mu$m particles). (b) The effect of the finite particle size distribution becomes evident, best fit of the data to eqs 10 and 14.

Introducing a particle size distribution function $f(r_p)$, where $f(r_p)dr_p$ is the fraction of particles having a radius in the range $(r_p + dr_p)$, the appropriate expression for describing diffusion out of the spherical particles is

$$\frac{A_{intra}(\Delta)}{A_{intra}(0)} = \frac{6}{\pi^2}\sum_{n=1}^{\infty}\frac{1}{n^2}\int_{r_p=0}^{\infty} f(r_p)\exp\left[-n^2\pi^2\frac{D_{intra}\Delta}{r_p^2}\right]dr_p \qquad (13)$$

The particle size distributions of the supports have been measured and particle sizes were found to be normally (Gaussian) distributed. When $\mu$ and $\sigma$, respectively, denote the mean and standard deviation of the particle radius, eq 13 then becomes[102]

$$\frac{A_{intra}(\Delta)}{A_{intra}(0)} = \frac{6}{\sigma\pi^2\sqrt{2\pi}}\sum_{n=1}^{\infty}\frac{1}{n^2}\int_{r_p=0}^{\infty}\times \exp\left[-\left(\frac{r_p-\mu}{\sigma\sqrt{2}}\right)^2 - n^2\pi^2\frac{D_{intra}\Delta}{r_p^2}\right]dr_p \qquad (14)$$

**TABLE 4: Exchange Kinetics $B = D_{intra}\pi^2/r_p^2$ and $D_{intra}$ for Water**

| parameter | material | | |
|---|---|---|---|
| | YMC ODS-A S50 | POROS 50 R2 | SOURCE 30Q |
| $B$ (eq 10) | 11.51 | 19.11 | 35.48 |
| $B$ (eq 11)[a] | 11.94 | 19.54 | *e* |
| $B$ (eq 12)[b] | 8.62 | 16.47 | 35.53 |
| $D_{intra}$ [$10^{-5}$ cm$^2$/s], eq 10[c] | 0.73 | 1.21 | 0.81 |
| $D_{intra}$ [$10^{-5}$ cm$^2$/s], eq 14[d] | 0.80 | 1.30 | 0.83 |

[a] For $A_{intra}(\Delta)/A_{intra}(0) > 0.45$. [b] For $0 < A_{intra}(\Delta)/A_{intra}(0) < 0.15$. [c] Based on the mean particle radius alone. [d] Using the mean particle radius and its standard deviation (cf. Table 1). [e] The initial part of the mass transfer data is missing due to the smaller particle size and the lower limit of the observation times.

**TABLE 5: $D_{intra}$ from Exchange Kinetics and Steady-State Pore Diffusion**

| parameter | YMC ODS-A S50[a] | | POROS 50 R2[a] | | SOURCE 30Q[a] | |
|---|---|---|---|---|---|---|
| | $H_2O$[b] | $CH_3CN$[b] | $H_2O$[b] | $CH_3CN$[b] | $H_2O$[b] | $CH_3CN$[b] |
| $D_{intra}$ [$10^{-5}$ cm$^2$/s], eq 14 | 0.80 | 1.45 | 1.30 | 2.18 | 0.83 | 1.48 |
| $D_{intra}$ [$10^{-5}$ cm$^2$/s], Table 2 | 0.96 | 1.67 | 1.46 | 2.46 | 1.03 | 1.77 |
| $\delta_{film}$ [$\mu$m] | 2.2 | 1.9 | 1.7 | 1.7 | 1.6 | 1.4 |
| $\delta_{film}/d_p$ | 0.044 | 0.038 | 0.034 | 0.034 | 0.052 | 0.046 |
| Pe[c] | 491 | 275 | 491 | 275 | 177 | 99 |

[a] Material. [b] Fluid. [c] Pe = particle Peclet number $= 4F_v d_p/(\epsilon_{inter}\pi d_c^2 D_m)$, with $\epsilon_{inter}$, the interparticle porosity (assumed 0.38) and $d_c$, the column diameter (0.46 cm).

With the information about $\mu$ and $\sigma$, obtained by means of independent measurements, eq 14 was evaluated numerically and an indeed excellent agreement with the experimental data could be established (Figure 4b). The values of $D_{intra}$ obtained by this procedure (eq 14) are also given in Table 4.

Thus, by taking proper account of the supports particle size distribution (and the shape), a very satisfactory quantitative description of the experimental mass transfer data may be obtained from the diffusion equation, and for the moderate particle size distributions encountered in this work, already eq 10 provides a good working definition of the intraparticle diffusivity. With the monodisperse particles hardly any error is introduced in the determination of $D_{intra}$ by assuming a uniform particle size (eq 10). For the other two supports, the effect of the broader size distribution leads to an upward correction of $D_{intra}$ of the order of 8%. These particle size distributions are still representative for today's high-performance packings where the distributions tend to be no wider than about 25% around the mean.[61] The results are in agreement with theoretical analyses on this topic,[103,104] which indicate that the particle size distribution has a significant influence on chromatographic performance only for much broader or asymmetric distributions.

The same series of measurements and calculations reported for water (Figure 4 and Table 4) were also made using acetonitrile as the mobile phase, with similar results. These values of $D_{intra}$ for water and acetonitrile (eq 14), together with the corresponding data obtained from the steady-state pore diffusion measurements (Table 2) are summarized in Table 5. It is now instructive to compare the agreement between these two sets of $D_{intra}$ values because they necessarily have to be consistent in terms of the inherently associated fluid dynamics, network topology and particle dimensions.

**Comparison between Steady-State and Transient Measurements.** There exists a fair qualitative agreement between these two approaches, but it becomes evident that the intraparticle diffusivities based on the exchange kinetics are systematically smaller (between 10 and 20%), even though these data have been corrected for the effects of the particle size distribution. In turn, the particles shape or size distribution does not influence the values of $D_{intra}$ which are calculated from the steady-state pore diffusion measurement, because the rms translational displacement of the stagnant fluid over time $\Delta$ is here directly measured (cf. Figure 1 and eq 7). Thus, the latter values of $D_{intra}$ represent the time-weighted average of the fluid molecules in stagnant regions of the packed bed. On the other hand, the values of $D_{intra}$ extracted from the mass transfer curves are based on the predetermination of the stagnant fluid fractions over times $\Delta$, which represent the volume-weighted average of fluid molecules in (any) stagnant regions of the packed bed, and $D_{intra}$ is then obtained from the decay rate of these curves (using eq 10 or 14). Included in these data, $A_{intra}(\Delta)/A_{intra}(0)$ vs $\Delta$ (Figure 4), is the contribution of the stagnant boundary layer which exists under laminar flow conditions at the particles external surface.[5,13] When the fluid molecules diffuse out of the particles and reach the spheres boundaries they first move through this stagnant film, where the transport normal to the surface is dominated by diffusion,[4] before they enter the flow streamlines. The effect of the boundary layer, an idealized stagnant, spherically symmetric film, is to slightly enlarge each particle.[9]

Considering the effect of the stagnant boundary layer on the time-weighted average value of $D_{intra}$, any influence is due to the higher value of the diffusivity within this film ($D_{film} \approx D_m$) compared to the situation in the intraparticle pore space ($D_{intra} = D_m/\tau_{intra}$). Following a fluid molecule from the center of the spherical particle to its external surface, a characteristic time $\Delta_{intra}$ of 325 ms is calculated based on eq 6 for travelling this net distance of $r_p$ (using water and the porous C18 silica particles as an example, $d_p = 50$ $\mu$m and $\tau_{intra} = 2.24$). Assuming a film thickness of 2.0 $\mu$m ($0.04d_p$), the time $\Delta_{film}$ it takes the fluid molecules to pass this stagnant boundary layer (moving normal to the particle surface) is less than 1 ms ($D_m = 2.15 \times 10^{-5}$ cm$^2$/s). When each stagnant fluid molecule has enough time to sample both the intraparticle pore space and the film region, the time-weighted average of the diffusion coefficients $D_{stag}$ of the stagnant fluid can be expressed as

$$D_{stag} = \frac{\sum_n D_n \Delta_n}{\sum_n \Delta_n} = \frac{(D_{intra}\Delta_{intra}) + (D_{film}\Delta_{film})}{\Delta_{intra} + \Delta_{film}} \cong D_{intra} \qquad (15)$$

Using for $D_n$ and $\Delta_n$ the values calculated in the above example, we find $D_{stag} = 1.0038D_{intra}$. Unfortunately, this

situation corresponds to observation times where the stagnant mobile phase mass transfer becomes already complete, because in terms of probability, fluid molecules originally located at the center of the particle must also be able to reach the stagnant boundary layer so that eq 15 can be applied (i.e., $\Delta \approx \Delta_{intra} = \Delta_e$, eq 6). But even at the shorter observation times, where the effective, intraparticle self-diffusion coefficients are typically measured (cf. Figure 2), a similar dimensional consideration shows that $D_{stag} \approx D_{intra}$ to within 1.5%. Thus, the influence of the slightly different diffusivity experienced by the fluid molecules in the stagnant film enveloping the spheres on the determined values of the steady-state intraparticle diffusivities (given in Table 2 in form of the respective tortuosity factors) can be neglected.

The situation is different for the reported transient measurements. The volumetric effect of the stagnant boundary layer manifests itself in an additional (diffusional) mass transfer resistance external to the spheres. Thus, the actually stagnant interstitial fluid in the packed bed at a given Peclet number dictates an effective interparticle porosity available for flow.[5] On the other hand, the mean particle radius enters in eqs 10 and 14 as a squared "constant". From an intraparticle viewpoint, this immediately suggests the introduction of a hydrodynamically effective particle radius (including the film thickness $\delta_{film}$) to account for its contribution to the recorded mass transfer kinetics. It certainly represents an oversimplified picture of the (considerably streamlined) stagnant fluid at the free surface of the particles and in the cusp regions around their contact points, but nevertheless provides a tractable starting point within this study to cover the average effect.

For the calculation of the data reported in Tables 4 and 5, the mean particle radius was used as determined from the particle size distribution measurement. Now, the accurate values of the steady-state pore diffusivities act as a boarder line for $D_{intra}$ and the systematically lower diffusivities obtained from the exchange kinetics are adjusted to these numbers by defining the hydrodynamically effective particle radius, $r_p^* = r_p + \delta_{film}$, i.e., the steady-state diffusivities (Table 2) are used as input parameters in eq 14 and the ("effective") mean particle radius, with $\mu = r_p^*$, is fitted. The values of $\delta_{film}$ obtained by this procedure are listed in Table 5. The measurements were made at a volumetric flow rate, $F_v$, of 8.0 mL/min in case of the 50 $\mu$m particles and at one of 4.8 mL/min with the smaller 30 $\mu$m particles due to a higher column pressure drop in this case. The corresponding (particle) Peclet numbers of each experiment are also given in Table 5. Depending on the actual hydrodynamic conditions, we find a film thickness for the different fluid phases and support particles ranging between 1.4 and 2.2 $\mu$m (i.e., up to $0.05d_p$). These data are now inspected in view of their dimension, but they are too limited to allow conclusions about the dependence of the stagnant boundary layer thickness on molecular diffusivity ($H_2O$ and $CH_3CN$) and Peclet number. Compared to the 50 $\mu$m particles, the results obtained for the 30 $\mu$m spheres (Table 5, $\delta_{film}/d_p$), however, indicate that the boundary layer is thicker at lower Peclet numbers.

The flow rate dependence (above Pe $\approx$ 50) of its thickness is an important criterion for the existence of a stagnant boundary at the interface. To confirm this observation, we conducted experiments at different flow rates and carefully recorded the complete mass transfer kinetics with purely diffusive particles. This ensures that the intraparticle diffusivity itself will be independent of Pe (cf. Figure 3a) and any significant differences in the observed exchange kinetics may then be traced back to a change in the hydrodynamically effective particle diameter. Figure 5 shows the results for acetonitrile in the column packed with the 50 $\mu$m C18 silica particles. The parameters obtained

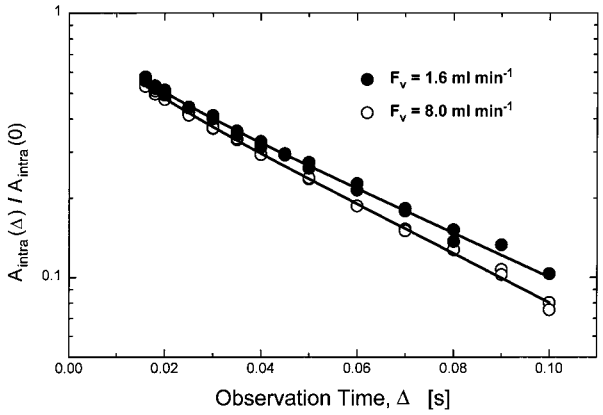


**Figure 5.** Influence of the flow rate on the diffusion-limited exchange kinetics. Mobile phase, pure acetonitrile. Column packed with porous C18 silica particles (YMC ODS-A S50). Best fit of the data to eq 14 (solid line).

with eqs 10 and 14 are summarized in Table 6. As may be seen, the flow rate probably has an effect and the value of $D_{intra}$ apparently increases steadily when the mean particle radius is maintained strictly constant at its value obtained from the particle size distribution measurement.

The same kind of observation has already been made by Boyd et al.[9] in their classical work on the kinetics of ion exchange adsorption processes in a shallow-bed apparatus. For their diffusion-limited stagnant mobile phase mass transfer kinetics these authors found a clear dependence on the flow rate of the "constant" $B = D_{intra}\pi^2/r_p^2$ in eq 10. They concluded that the particles were made effectively slightly larger by a surrounding liquid film which should be an inverse function of the flow velocity.

Thus, by keeping now in our calculations the acetonitrile intraparticle diffusivity constant at its value known from the steady-state pore diffusion measurement ($D_{intra} = 1.67 \times 10^{-5}$ cm$^2$/s), the increase in Peclet number is accompanied by a steady decrease of the film thickness from 3.1 to 1.9 $\mu$m ($r_p^*$ from 28.2 to 27.0 $\mu$m, Table 6). Due to the dimensions inherently involved (50 and 30 $\mu$m particles), the absolute effects are expectedly small. We now seek for dimensional estimates of the boundary layer and its dependence on the hydrodynamics available from literature data.

In an attempt to describe the interplay of convective and diffusional mixing of unsorbed solutes in the interstitial space of packed beds, Horváth and Lin[105] argued that eddy dispersion occurs only outside the stagnant film, i.e., in the liquid which is actually moving between the particles. To evaluate the thickness of this film they came up with the "free surface model" of Pfeffer and Happel[106,107] who developed it in their analytical study of heat and mass transfer to a bed of spherical particles at low Reynolds numbers. These authors found that at high Peclet (Pe) numbers the Sherwood (Sh) number depends on Pe by

$$\mathrm{Sh} \equiv \frac{k_{film} d_p}{D_m} = \Omega \mathrm{Pe}^{1/3} \qquad (16)$$

Here, $k_{film}$ is the fluid film mass transfer coefficient and the value of $\Omega$ is a function of the interstitial porosity only, changing from 3.6 to 3.2 when $\epsilon_{inter}$ varies from 0.36 to 0.42. Fair agreement with this dependence has been obtained by Wilson and Geankoplis[108] on the basis of their electrochemical measurements (for $0.0016 < \mathrm{Re} < 55$).

**TABLE 6: Flow Rate Dependence of Mass Transfer Kinetics[a]**

| $F_v$ [ml/min] | Pe | $D_{intra}$ [$10^{-5}$ cm$^2$/s][b] | $r_p^* = r_p + \delta_{film}$ [$\mu$m][c] | $\delta_{film}/d_p$ | $B$[d] | $\delta_{film}$ [$\mu$m][e] |
|---|---|---|---|---|---|---|
| 1.6 | 55 | 1.34 | 28.2 | 0.062 | 19.2 | 3.7 |
| 4.1 | 141 | 1.42 | 27.3 | 0.044 | 20.9 | 2.7 |
| 8.0 | 275 | 1.45 | 27.0 | 0.038 | 21.3 | 2.2 |

[a] Mobile phase: acetonitrile. Packing material: 50 $\mu$m C18 silica (YMC ODS-A S50). [b] Calculated with eq 14, assuming a constant mean particle radius, $r_p = 25.1$ $\mu$m (Table 1). [c] Obtained from eq 14, using a constant diffusivity, $D_{intra} = 1.67 \times 10^{-5}$ cm$^2$/s (Table 2). [d] $B = D_{intra}\pi^2/r_p^2$, eq 10. [e] Based on eq 17, with $\Omega = 3.6$.

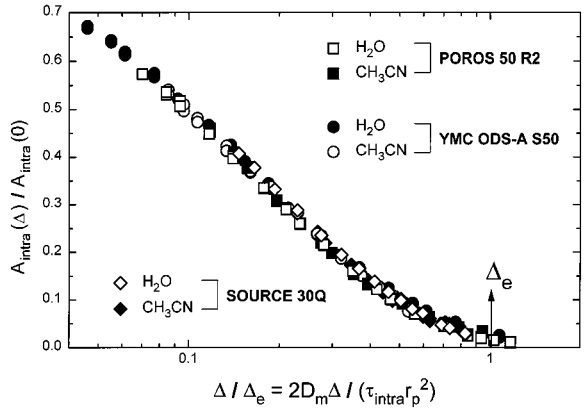


**Figure 6.** Total fraction of the stagnant fluid remaining unexchanged in the packed beds as a function of the observation time, normalized by the characteristic exchange time ($\Delta_e$). Mobile phases, water and acetonitrile. $F_v = 4.8$ mL/min (30 $\mu$m particles) and 8.0 mL/min (50 $\mu$m particles).

The film thickness was then obtained by relating it to the mass transfer coefficient via the Nernst diffusion layer[105]

$$\delta_{film} = \frac{D_m}{k_{film}} = \frac{d_p}{\Omega Pe^{1/3}} \qquad (17)$$

The stagnant boundary layer thickness expected on the basis of eq 17 (strictly applicable for Pe > 50) is given in Table 6 for comparison. Although the absolute values of the film thickness obtained from our measurements are found to diverge from the calculated ones by up to 20%, they still fall into a reasonable order of magnitude and follow qualitatively the predictions of eq 17. It should be pointed out that at this stage and with the available data such a comparison should help to gain dimensional insight, rather than providing quantitative description or agreement.

Thus, by introducing a flow rate dependent, effective particle radius, which is similar to the definition of an effective (velocity dependent) interparticle porosity, the PFG-NMR approach appears promising to study the (relative) hydrodynamic behavior of the interstitial stagnant fluid volume in packed beds of porous particles. (N.B. For the sake of completeness, it has been pointed out correctly that the film mass transfer coefficient used by Horváth and Lin[105] was originally derived under conditions of a concentration boundary layer profile.[109] The correct film thickness thus would be the concentration boundary layer thickness which will be less than the Nernst diffusion layer thickness.)

Finally, we close by returning to the topological aspect of the intraparticle pore network. All mass transfer data recorded for the three packing materials are plotted in Figure 6 against the observation time which now has been normalized by the characteristic exchange time defined by eq 6. In the calculation for $\Delta_e$ the intraparticle tortuosity factors obtained from the steady-state pore diffusion measurement (Table 2) have been used. The exchange kinetics obtained for the small, nonsorbed fluid molecules in the different pore networks collapse onto a single decay curve characteristic of Fickian diffusion. It demonstrates that in this case simple geometrical aspects (particle shape, mean diameter, particle size distribution, and the tortuosity factor) are the only important parameters which characterize the stagnant mobile phase mass transfer resistance. In this respect, the results indicate again the importance of the actual correlation (or randomness) of pore interconnectivity in the particles.

## Conclusions

The PFG-NMR approach followed in this work allows to record two series of data with complementary character regarding the diffusion and exchange kinetics in chromatographic media. The steady-state pore diffusion measurement gives an effective, intraparticle self-diffusion coefficient from which the respective tortuosity factor can be calculated. The results demonstrate the profound effect of the actual correlation of interconnectivity between different pore sizes and thereby achieved hierarchy in pore structure on the associated transport behavior. It has a strong impact on the chromatographic performance of the support. These data are independent of the actual packing quality of particles in the column, their shape or size distribution, and external contributions due to the stagnant boundary layer.

The observational time scale of the PFG-NMR method can also be used to record the complete stagnant mobile phase mass transfer kinetics in the packed bed of porous particles. These data are influenced by the respective particle shape and size distribution, and by the hydrodynamics of the stagnant boundary layer (consequently, also by the packing density), which presents diffusional mass transfer resistance external to the particles. The effects of the particle shape and size distribution can be accounted for by independent measurements and the diffusion equation provides an excellent quantitative description of the exchange kinetics including this information. Slight corrections (<10%) of the intraparticle diffusivity are found for moderate Gaussian particle size distributions. The remaining effect of the stagnant boundary layer can be accounted for by the introduction of a hydrodynamically effective particle diameter, which is found to depend on Peclet number.

The approach shows potential to study and differentiate between the mechanisms that may contribute to the mass transfer in porous particles. This points toward enhanced surface diffusion and intraparticle-forced convection, which both may be responsible for higher effective, intraparticle diffusivities than those within the tortuosity limited regime (i.e., $D_{intra} < D_m$ and $\tau_{intra} > 1$) encountered in this work. Further, the kinetics of adsorption/desorption could be derived more accurately if we correct properly for the intraparticle diffusivity contribution. Thus, it will be extremely useful to carry out similar determinations on a variety of other relevant chromatographic and ion exchange media.

**Acknowledgment.** One of the authors (U. T.) gratefully acknowledges the award of a Marie Curie Fellowship under

the Training and Mobility of Researchers (TMR) Program from the European Union (Contract ERBFMBI-CT98-3437).

## References and Notes

(1) Giddings, J. C. *Dynamics of Chromatography*; Marcel Dekker: New York, 1965.
(2) Weber, S. G.; Carr, P. W. *The Theory of the Dynamics of Liquid Chromatography*. In *High Performance Liquid Chromatography*; Brown, P. R., Hartwick, R. A., Eds.; Wiley: New York, 1989; Chapter 1.
(3) Dullien, F. A. L. *Porous Media: Fluid Transport and Pore Structure*; Academic Press: New York, 1992.
(4) King, C. V. *J. Am. Chem. Soc.* **1935**, *57*, 828.
(5) Gottschlich, C. F. *AIChE J.* **1963**, *9*, 88.
(6) Deans, H. A.; Lapidus, L. *AIChE J.* **1960**, *6*, 656.
(7) Ergun, S. *Chem. Eng. Prog.* **1952**, *48*, 227.
(8) Martin, A. J. P.; Synge, R. L. M. *Biochem. J.* **1941**, *35*, 1358.
(9) Boyd, G. E.; Adamson, A. W.; Meyers, L. S., Jr. *J. Am. Chem. Soc.* **1947**, *69*, 2836.
(10) Boyd, G. E.; Meyers, L. S., Jr.; Adamson, A. W. *J. Am. Chem. Soc.* **1947**, *69*, 2849.
(11) Klinkenberg, A.; Sjenitzer, F. *Chem. Eng. Sci.* **1956**, *5*, 258.
(12) van Deemter, J. J.; Zuiderweg, F. J.; Klinkenberg, A. *Chem. Eng. Sci.* **1956**, *5*, 271.
(13) Rosen, J. B. *Ind. Eng. Chem.* **1954**, *46*, 1590.
(14) Done, J. N.; Knox, J. H. *J. Chromatogr. Sci.* **1972**, *10*, 606.
(15) Huber, J. F. K. *Ber. Bunsen-Ges. Phys. Chem.* **1973**, *77*, 179.
(16) Horváth, Cs.; Lin, H.-J. *J. Chromatogr.* **1978**, *149*, 43.
(17) Unger, K. K.; Jilge, G.; Kinkel, J. N.; Hearn, M. T. W. *J. Chromatogr.* **1986**, *359*, 61.
(18) Kirkland, J. J. *Anal. Chem.* **1992**, *64*, 1239.
(19) Kalghatgi, K.; Fellegvári, I.; Horváth, Cs. *J. Chromatogr.* **1992**, *604*, 47.
(20) Hjertén, S.; Liao, J.-I.; Zhang, R. *J. Chromatogr.* **1989**, *473*, 273.
(21) Petro, M.; Svec, F.; Gitsov, I.; Fréchet, J. M. J. *Anal. Chem.* **1996**, *68*, 315.
(22) Reeder, D. H.; Clausen, A. M.; Annen, M. J.; Flickinger, M. C.; Carr, P. W.; McCormick, A. V. *J. Colloid Interface Sci.* **1996**, *184*, 328.
(23) Afeyan, N. B.; Gordon, N. F.; Mazsaroff, I.; Varady, L.; Fulton, S. P.; Yang, Y. B.; Regnier, F. E. *J. Chromatogr.* **1990**, *519*, 1.
(24) Frey, D. D.; Schweinheim, E.; Horváth, Cs. *Biotechnol. Prog.* **1993**, *9*, 273.
(25) Nir, A.; Pismen, L. M. *Chem. Eng. Sci.* **1977**, *32*, 35.
(26) Rodrigues, A. E.; Lopes, J. C.; Lu, Z. P.; Loureiro, J. M.; Dias, M. M. *J. Chromatogr.* **1992**, *590*, 93.
(27) Heeter, G. A.; Liapis, A. I. *J. Chromatogr. A* **1997**, *761*, 35.
(28) Davis, R. H.; Stone, H. A. *Chem. Eng. Sci.* **1993**, *48*, 3993.
(29) Satterfield, C. N.; Colton, C. K.; Pitcher, W. H., Jr. *AIChE J.* **1973**, *19*, 628.
(30) Limbach, K. W.; Wei, J. *AIChE J.* **1990**, *36*, 242.
(31) Epstein, N. *Chem. Eng. Sci.* **1989**, *44*, 777.
(32) Yau, W. W.; Kirkland, J. J.; Bly, D. D. *Modern Size-Exclusion Liquid Chromatography*; John Wiley & Sons: New York, 1979; Chapter 2.
(33) Giddings, J. C.; Kucera, E.; Russel, C. P.; Myers, M. N. *J. Phys. Chem.* **1968**, *72*, 4397.
(34) Satterfield, C. N. *Mass Transfer in Heterogeneous Catalysis*; MIT Press: Cambridge, MA, 1970.
(35) Burganos, V. N.; Sotirchos, S. V. *AIChE J.* **1987**, *33*, 1678.
(36) Carberry, J. J.; Bretton, R. H. *AIChE J.* **1958**, *4*, 367.
(37) Aris, R. *Chem. Eng. Sci.* **1959**, *11*, 194.
(38) Koch, D. L.; Brady, J. F. *J. Fluid Mech.* **1985**, *154*, 399.
(39) Deans, H. A. *Soc. Pet. Eng. J.* **1963**, *3*, 49.
(40) Coats, K. H.; Smith, B. D. *Soc. Pet. Eng. J.* **1964**, *4*, 73.
(41) Sahimi, M.; Tsotsis, T. T. *J. Catal.* **1985**, *96*, 552.
(42) Hollewand, M. P.; Gladden, L. F. *Chem. Eng. Sci.* **1992**, *47*, 1761.
(43) Coffman, J. L.; Lightfoot, E. N.; Root, T. W. *J. Phys. Chem. B* **1997**, *101*, 2218.
(44) Li, J.; Cantwell, F. F. *J. Chromatogr. A* **1996**, *726*, 37.
(45) Li, J.; Litwinson, L.; Cantwell, F. F. *J. Chromatogr. A* **1996**, *726*, 25.
(46) Villermaux, J. *J. Chromatogr. Sci.* **1974**, *12*, 822.
(47) Haynes, H. W., Jr. *Catal. Rev.−Sci. Eng.* **1988**, *30*, 563.
(48) Ding, A.; Candela, D. *Phys. Rev. E* **1996**, *54*, 656.
(49) Tallarek, U.; Albert, K.; Bayer, E.; Guiochon, G. *AIChE J.* **1996**, *42*, 3041.
(50) Lebon, L.; Oger, L.; Leblond, J.; Hulin, J. P.; Martys, N. S.; Schwartz, L. M. *Phys. Fluids* **1996**, *8*, 293.
(51) Seymour, J. D.; Callaghan, P. T. *AIChE J.* **1997**, *43*, 2096.
(52) Tessier, J. J.; Packer, K. J.; Thovert, J.-F.; Adler, P. M. *AIChE J.* **1997**, *43*, 1653.
(53) Amin, M. H. G.; Gibbs, S. J.; Chorley, R. J.; Richards, K. S.; Carpenter, T. A.; Hall, L. D. *Proc. R. Soc. A* **1997**, *453*, 489.
(54) Tallarek, U.; van Dusschoten, D.; Van As, H.; Bayer, E.; Guiochon, G. *J. Phys. Chem. B* **1998**, *102*, 3486.
(55) Tessier, J. J.; Packer, K. J. *Phys. Fluids* **1998**, *10*, 75.
(56) Stapf, S.; Packer, K. J.; Graham, R. G.; Thovert, J.-F.; Adler, P. M. *Phys. Rev. E* **1998**, *58*, 6206.
(57) Tallarek, U.; Bayer, E.; Guiochon, G. *J. Am. Chem. Soc.* **1998**, *120*, 1494.
(58) Tallarek, U.; Bayer, E.; van Dusschoten, D.; Scheenen, T.; Van As, H.; Guiochon, G.; Neue, U. D. *AIChE J.* **1998**, *44*, 1962.
(59) Hollewand, M. P.; Gladden, L. F. *Chem. Eng. Sci.* **1995**, *50*, 309.
(60) Tallarek, U.; van Dusschoten, D.; Van As, H.; Guiochon, G.; Bayer, E. *Angew. Chem.* **1998**, *110*, 1983; *Angew. Chem., Int. Ed. Engl.* **1998**, *37*, 1882.
(61) Neue, U. D. *HPLC Columns: Theory, Technology, and Practice*; Wiley-VCH: New York, 1997.
(62) Poole, C. F.; Poole, S. K. *Chromatography Today*; Elsevier: Amsterdam, 1993.
(63) Schenck, J. F. *Med. Phys.* **1996**, *23*, 815.
(64) Regnier, F. E. *Nature* **1991**, *350*, 634.
(65) Ugelstad, J.; Soderberg, L.; Berge, A.; Bergstrom, J. *Nature* **1983**, *303*, 95.
(66) Stejskal, E. O.; Tanner, J. E. *J. Chem. Phys.* **1965**, *42*, 288.
(67) Stejskal, E. O. *J. Chem. Phys.* **1965**, *43*, 3597.
(68) Callaghan, P. T. *Principles of Nuclear Magnetic Resonance Microscopy*; Clarendon Press: Oxford, 1993; Chapter 6.3.
(69) Kärger, J.; Heink, W. *J. Magn. Reson.* **1983**, *51*, 1.
(70) Callaghan, P. T.; Coy, A.; MacGowan, D.; Packer, K. J.; Zelaya, F. O. *Nature* **1991**, *351*, 467.
(71) Callaghan, P. T.; MacGowan, D.; Packer, K. J.; Zelaya, F. O. *J. Magn. Reson.* **1990**, *90*, 177.
(72) Cotts, R. M. *Nature* **1991**, *351*, 443.
(73) Zimmerman, J. R.; Brittin, W. E. *J. Phys. Chem.* **1957**, *61*, 1328.
(74) Brownstein, K. R.; Tarr, C. E. *Phys. Rev. A* **1979**, *19*, 2446.
(75) Stilbs, P. *Prog. Nucl. Magn. Reson. Spectrosc.* **1987**, *19*, 1.
(76) Kärger, J.; Pfeifer, H.; Heink, W. *Adv. Magn. Reson.* **1988**, *12*, 1.
(77) Nawrocki, J. *Chromatographia* **1991**, *31*, 177.
(78) Albright, J. G.; Mills, R. *J. Phys. Chem.* **1965**, *69*, 3120.
(79) Reyes, S. C.; Iglesia, E. *J. Catal.* **1991**, *129*, 457.
(80) Hollewand, M. P.; Gladden, L. F. *Chem. Eng. Sci.* **1992**, *47*, 2757.
(81) Nicholson, D.; Petrou, J. K.; Petropoulos, J. H. *Chem. Eng. Sci.* **1988**, *43*, 1385.
(82) Petropoulos, J. H.; Liapis, A. I.; Kolliopoulos, N. P.; Petrou, J. K.; Kanellopoulos, N. K. *Bioseparation* **1990**, *1*, 69.
(83) Petropoulos, J. H.; Petrou, J. K.; Liapis, A. I. *Ind. Eng. Chem. Res.* **1991**, *30*, 1281.
(84) Sharratt, P. N.; Mann, R. *Chem. Eng. Sci.* **1987**, *42*, 1565.
(85) Carman, P. C. *Trans. Inst. Chem. Eng. (London)* **1937**, *15*, 150.
(86) Feng, C.; Stewart, W. E. *Ind. Eng. Chem. Fundam.* **1973**, *12*, 143.
(87) Venema, P.; Struis, R. P. W. J.; Leyte, J. C.; Bedeaux, D. *J. Colloid Interface Sci.* **1991**, *141*, 360.
(88) Blees, M. H.; Leyte, J. C. *J. Colloid Interface Sci.* **1994**, *166*, 118.
(89) Dunn, K.-J.; Bergman, D. J. *J. Chem. Phys.* **1995**, *102*, 3041.
(90) Pfeiffer, J. F.; Chen, J. C.; Hsu, J. T. *AIChE J.* **1996**, *42*, 932.
(91) Guiochon, G.; Golshan-Shirazi, S.; Katti, A. M. *Fundamentals of Preparative and Nonlinear Chromatography*; Academic Press: Boston, MA, 1994.
(92) Lorenzano-Porras, C. F.; Carr, P. W.; McCormick, A. V. *J. Colloid Interface Sci.* **1994**, *164*, 1.
(93) Lorenzano-Porras, C. F.; Annen, M. J.; Flickinger, M. C.; Carr, P. W.; McCormick, A. V. *J. Colloid Interface Sci.* **1995**, *170*, 299.
(94) Gibbs, S. J.; Lightfoot, E. N.; Root, T. W. *J. Phys. Chem.* **1992**, *96*, 7458.
(95) Lightfoot, E. N.; Athalye, A. M.; Coffman, J. L.; Roper, D. K.; Root, T. W. *J. Chromatogr. A* **1995**, *707*, 45.
(96) Rigby, S. P.; Gladden, L. F. *Chem. Eng. Sci.* **1996**, *51*, 2263.
(97) Liapis, A. I.; McCoy, M. A. *J. Chromatogr.* **1992**, *599*, 87.
(98) Rodrigues, A. E.; Ahn, B.; Zoulalian, A. *AIChE J.* **1982**, *28*, 541.
(99) Crank, J. *The Mathematics of Diffusion*; Clarendon Press: Oxford, 1956; Chapter 6.
(100) Carslaw, H. S.; Jaeger, J. C. *Conduction of Heat in Solids*; Clarendon Press: Oxford, 1959; Chapter 9.3.
(101) Westrin, B. A.; Zacchi, G. *Chem. Eng. Sci.* **1991**, *46*, 1911.
(102) Ruthven, D. M.; Loughlin, K. F. *Chem. Eng. Sci.* **1971**, *26*, 577.
(103) Rasmuson, A. *Chem. Eng. Sci.* **1985**, *40*, 621.
(104) Lin, Y. S.; Ma, Y. H. *AIChE J.* **1990**, *36*, 1569.
(105) Horváth, Cs.; Lin, H.-J. *J. Chromatogr.* **1976**, *126*, 401.
(106) Pfeffer, R.; Happel, J. *AIChE J.* **1964**, *10*, 605.
(107) Pfeffer, R. *Ind. Eng. Chem. Fundam.* **1964**, *3*, 380.
(108) Wilson, E. J.; Geankoplis, C. J. *Ind. Eng. Chem. Fundam.* **1966**, *5*, 9.
(109) Arnold, F. H.; Blanch, H. W.; Wilke, C. R. *J. Chromatogr.* **1985**, *330*, 159.